Spiral wave dynamics under feedback via an equilateral triangular sensory domain

Somprasong Naknaimueang,[1] Michael A. Allen,[2,*] and Stefan C. Müller[1]
[1]*Institut für Experimentelle Physik, Otto-von-Guericke-Universität Magdeburg, Universitätplatz 2, D-39106 Magdeburg, Germany*
[2]*Physics Department, Mahidol University, Rama 6 Road, Bangkok 10400, Thailand*
(Received 9 February 2006; published 29 December 2006)

We perform a numerical study of the trajectories of spiral wave cores in excitable systems whose excitability is modulated in proportion to the integral of the activity in a sensory domain in the shape of an equilateral triangle. As a result of this domain shape having vertices opposite sides, unusual forms of lobed limit cycles occur, which are destroyed and then re-form as the domain size is varied. Some key results are also demonstrated experimentally using the light-sensitive Belousov-Zhabotinsky reaction. To characterize the observed behavior, we introduce the concept of express and stagnation zones, which are regions where the trajectory moves particularly rapidly or slowly. The location and strength of the zones far from the domain are accounted for by approximating the parts of the spiral wave crossing the domain by a series of plane waves.

DOI: 10.1103/PhysRevE.74.066209 PACS number(s): 05.45.−a, 05.65.+b, 47.54.−r, 82.40.Bj

I. INTRODUCTION

Reaction-diffusion equations admitting stable pulse-shaped traveling wave solutions in one dimension will also exhibit spiral waves in two dimensions. The classic example of such equations are those governing excitable systems. In the spatially homogeneous state, an excitable system has, in addition to a single stable equilibrium, a transient attractor (the excited state) and a transient repellor (the threshold). The peak of a wave in a spatially extended system corresponds to the transient attractor. Excitable systems in nature in which spiral waves have been observed include the Belousov-Zhabotinsky (BZ) reaction [1], catalytic oxidation on surfaces [2], slime mold [3], heart muscle [4], and mammalian neocortex [5].

Of particular interest is the motion of the spiral tip as the spiral wave front propagates. If the parameters of the excitable system are held fixed both temporally and spatially, the tip trajectory is, in general, a cycloid [6]. However, as a limiting case, depending on the system and the choice of parameters, it is possible to obtain rigid rotation whereby the tip trajectory is circular (and is referred to as the spiral core) and the spiral wave maintains a constant shape. If a system parameter that affects the excitability is varied periodically in time, in addition to cycloids, tip trajectories in the form of "wavy cycloids" and Lissajous figures are obtained [7–9].

The most striking long-term behavior of the tip is seen when the excitability is modulated via a feedback mechanism. In local feedback, an arbitrary point in the medium is selected and the excitability of the system is then modulated according to the state of the system at that measuring point. It is found that the trajectory of the spiral core center is attracted to a series of circular limit cycles centered on the measuring point [7]. If there is a sufficient time delay between the measurement and the subsequent modulation of the excitability, the limit cycles become unstable in favor of attractors of a more complicated nature [10].

The effect of various nonlocal feedback schemes has also been investigated. In this case, the excitability is modulated in response to the average value of the activity over a specified region of the system (the sensory domain). When the domain size is significantly smaller than the wavelength of the spiral wave, the spiral core trajectories are similar to those for local feedback. However, for larger domains, the nature of the attractors depends very much on the size and shape of the domain [11,12]. The change in behavior occurring as a function of domain size has been examined for circular [13] and square [11,14] domains. In this paper we present the results of a systematic computational study in the case of feedback control of rigidly rotating spiral waves using domains in the shape of an equilateral triangle. Some key results are also demonstrated experimentally using the light-sensitive BZ reaction.

The fact that for an equilateral triangular domain each vertex is opposite a side turns out to be crucial. It results in significant differences in the shape of the limit cycles and a more complicated sequence of bifurcations as compared with those obtained with a square domain. In the final part of the paper we use a simplified model to account for the locations of regions outside the domain where the core has an exceptionally large or small speed.

II. COMPUTATIONAL AND EXPERIMENTAL DETAILS

The excitable system we study numerically is governed by the equations

$$\frac{\partial u}{\partial t} = \nabla^2 u + F(u,v) - I(t), \quad \frac{\partial v}{\partial t} = \varepsilon G(u,v), \tag{1}$$

where u and v are the concentrations of activator and inhibitor, respectively, and the expressions for F and εG and the associated parameter values are those used in Ref. [11]. The feedback term $I(t)$ is given by

$$I(t) = I_0 + k_{\mathrm{fb}}(B(t) - B_0), \quad B(t) = \frac{1}{S}\int_D v(x,y,t)\,dx\,dy, \tag{2}$$

where S is the area of the sensory domain D over which the integration is performed, and B_0 is the average value of $B(t)$

*Corresponding author. Electronic address: frmaa@mahidol.ac.th

over one revolution of a spiral wave located at the center of the domain. We used $I_0=0$ and $k_{fb}=0.1$ throughout.

The numerical calculation was carried out using an adapted version of Barkley's program EZSPIRAL [15]. The code integrates (1) using the explicit Euler method with a nine-point Laplacian and no-flux boundary conditions, and also determines the location of the spiral tip. A time step of 0.05 and a space step of 0.5 were used throughout. A rigidly rotating spiral of pitch 70 space units that rotates about a core of radius 7 units is obtained by using the sector-shaped initial conditions specified in Ref. [16]. The discrepancy between our value of the pitch and that given in Refs. [11,17] of 64 in spite of our using identical parameter values is due to our using a larger time step and the nine-point rather than the five-point Laplacian. With time steps of less than 0.2 and 0.05, the nine- and five-point calculations give pitches of 66 and 64, respectively. After normalizing the length to units of wavelength the plots obtained from using the larger and smaller time steps were found to be essentially the same.

To aid interpretation of the numerical and experimental results, we also plot the drift vector field which depicts the drift velocity of the spiral core [11]. Following the method given in Ref. [11], the relative magnitude of the velocity is given by the magnitude of the first Fourier component of $B(t)$. The direction of the velocity is equal to $\phi+\phi_0$ where ϕ is the phase of the first Fourier component and ϕ_0 is a constant. We determine ϕ_0 by comparing the drift vector field with the path of the spiral core. In Ref. [11] the $B(t)$ needed for the drift vector plot was found by approximating the wave front as a thin Archimedean spiral. Instead, we use a fully formed spiral wave from the numerical solution of (1) without feedback. To exploit the threefold rotational symmetry about the triangle centroid, the drift vectors are evaluated on a triangular grid centered on this point for values of the polar angle in the range $0 \leqslant \theta < 120°$ only.

The drift vector fields we obtain for larger domain sizes are quite complex. Visualization of the flows and attractors is greatly enhanced by using the color of the arrows and background to indicate the sign of the divergence since attractors and repellors will occur in regions of negative and positive divergence, respectively. We use an inverse-magnitude scaled divergence obtained by dividing the divergence by the mean magnitude of the six vectors used to calculate the divergence. Coloring the background according to this scaled divergence makes regions where the magnitude of the vectors is low particularly striking.

The experimental observations were carried out using a photosensitive BZ reaction with a similar setup to previous studies [18,19]. The light-sensitive tris(2,2′-bipyridyl)ruthenium (II) catalyst, which gives rise to a decrease in the excitability of the system with increasing illumination, was present, immobilized at a concentration of 4.2 mM in a 0.33 ± 0.02 mm silica gel layer at the base of a 7-cm-diameter Petri dish. Two BZ solutions were prepared comprising $NaBrO_3$ (0.4, 0.17), H_2SO_4 (0.78, 1.56), malonic acid (0.336, 0.168), and NaBr (0.4, 0.2) where the respective molar concentrations are given in parentheses. After completion of the malonic acid bromination, 2 ml of the first solution was poured onto the gel from one side of the dish, followed by 8 ml of the second solution two minutes later. The reactants were uniformly illuminated from below using light from a Panasonic PT-L555E video projector controlled by a computer. Before reaching the dish, the light passes through a KG4 cool glass filter to eliminate radiant heat, a 310–530 nm BG6 filter, a ground glass plate to improve homogeneity, and a lens to collimate the beam. The light intensity used in the absence of feedback, I_0, was typically 1.0 W m^{-2}. Its value is chosen to ensure rigid rotation of the spiral waves, and was measured using a Tektronix J 1812 photometer put in place of the Petri dish. The experiments were conducted at an ambient temperature of 22 ± 1 °C and typically lasted 2–2.5 h, after which time the rigid rotation was lost due to depletion of the reactants.

To apply feedback to the system, the reaction is imaged every second using a Hamamatsu H 3077 charge-coupled device camera whose output is fed to a frame grabber card (DT 3155) for digitization. To facilitate the image processing, the contrast between wave front and background is enhanced by placing a 490 ± 13 nm filter in front of the camera. From the digitized image, a program computes the desired intensity level $I(t)$ according to (2) with v replaced by the image brightness. The feedback gain k_{fb}, held fixed for each experiment, is chosen to have a value of approximately 0.12 W m^{-2}/max($|B(t)-B_0|$). A signal is then sent to the frame grabber to update the projector intensity before the next image is taken.

Semicircular waves originate from the side of the dish where the first BZ solution is added. To generate a spiral wave, when the first wave front reaches the center (which occurs after the second solution has been added) half of it is removed by illumination with a high-intensity spot of light from a cold source (Schott, KL 1500). The remaining open-ended wave front evolves into a spiral wave near the center of the dish. The spiral is allowed to fully form before feedback is applied. An unperturbed spiral wave prepared in this way has an initial wavelength of between 2.1 and 3.0 mm and a period of 52–60 s. The spiral wavelength was monitored continually. In some cases it was found to increase and the tip trajectory from that point on was discarded.

III. COMPUTATIONAL AND EXPERIMENTAL RESULTS

Both the computational and experimental studies were carried out with clockwise spiral waves (which appear to rotate counterclockwise as the wave front propagates). The plots for counterclockwise spiral waves would be a mirror image of the ones presented here. From now on, all lengths are given in units of the spiral wavelength λ. The domain size d is defined as the length of a side of the triangle.

The behavior of the system is best characterized by considering the spiral core drift velocity vector field. The computational studies show that for d less than about 2, the centroid of the domain is a source. For d of around 1 or less, the source is surrounded by concentric, approximately circular, alternately stable and unstable limit cycles as is apparent from the drift vector plot of Fig. 1(a). From the vector plots in Figs. 1 and 2 it can be seen that, as d is increased, the innermost limit cycle decreases in size and becomes more triangular in shape. In all instances, the stable limit cycles

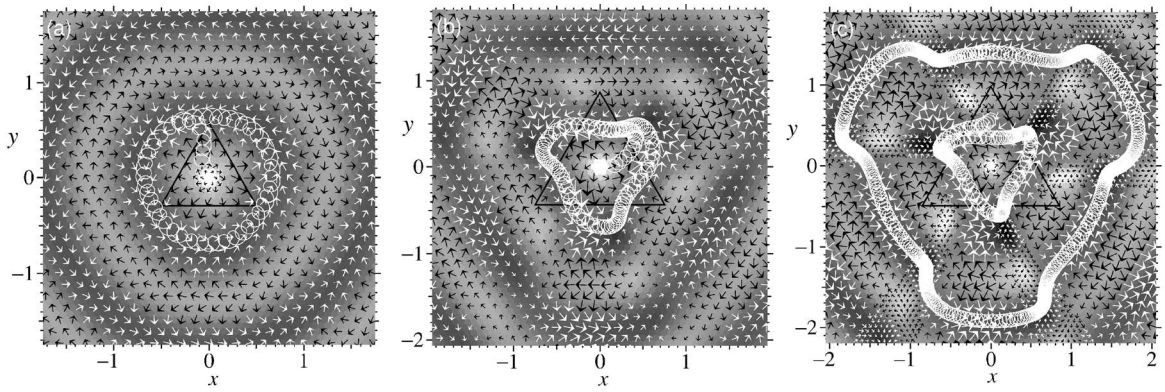

FIG. 1. Drift vector plots. In this and subsequent plots of this type, the black triangle is the domain, the white curves are the spiral tip paths, and the arrows indicate the drift velocity. The length of all but the small, narrow-headed arrows is proportional to the drift speed (although the proportionality constant differs for each plot). Black (white) arrows are in regions where the field divergence is positive (negative). The background is shaded according to the inverse-magnitude scaled divergence. Regions of negative (positive) divergence have a dark (light) background. d=(a) 1 and (b) 1.5. In (a) and (b) the tip trajectory starts near the central unstable focus and ends up on the innermost stable limit cycle. (c) d=1.7—tip trajectories are shown following the first two stable limit cycles.

flow counterclockwise, while the unstable limit cycles are in the opposite sense.

By around d=1.5, it is clear that there are regions where the spiral core speed is large and those where it is small, in addition to those near the single fixed point at the centroid. We refer to these as express and stagnation zones, respectively. Like the sinks and sources, the stagnation zones appear as the regions with the darkest or brightest background depending, respectively, on whether the divergence is negative or positive. Notice in Fig. 1(b) that the innermost limit cycle passes through three stagnation zones. It will be convenient to classify the express zones outside the domain according to the direction from the centroid in which they lie. Vertex express zones (VEZs) lie in the directions of the domain vertices, namely, θ=−30°, 90°, −150°, whereas lateral express zones (LEZs) are located in the opposing directions away from the centroid. Just outside the domain is an approximately hexagonal unstable limit cycle lying within six repelling express zones (three LEZs and three VEZs) interspersed with six stagnation zones. Further out there is a stable limit cycle of similar shape lying within six attracting express zones. As d increases further, the distance from the centroid to the VEZs decreases, while the corresponding distance to the LEZs increases. This results in the second stable limit cycle having three protruding lobes as can be seen in Fig. 1(c). We will refer to such lobed limit cycles as being of lateral or vertex type depending on whether the most protruding parts (the "lobes") are composed of LEZs or VEZs, respectively.

As a result of the increase in separation of the ends of the LEZs from the ends of the VEZs, the limit cycles become ever more distorted until by the time the domain size has reached d=1.8 the innermost unstable limit cycle has been destroyed via saddle-node bifurcations. The destruction of the lobed stable limit cycle surrounding it follows at just below d=1.82. With the two limit cycles destroyed, the basin of attraction for the central stable limit cycle becomes much larger—trajectories starting on and around the express zones that contained part of the destroyed lobed limit cycle will eventually make their way to it via a number of (negative divergence) stagnation zones. However, this extended basin is short lived. By d=1.85, a homoclinic bifurcation has occurred which results in the innermost LEZs no longer connecting with the central limit cycle but instead linking with the next attracting VEZs to form a vertex lobed stable limit cycle, as can be seen in Fig. 2. A further (lateral) lobed stable limit cycle passes through the second set of attracting VEZs. Trajectories starting on the attracting VEZs in between the second and third stable limit cycles will end in a sink. These sinks occur for only a small range of d. At d=1.86 this second set of VEZs is part of the basin of attraction for the third limit cycle, and by d=1.90, these VEZs make up part of the third stable limit cycle which is now vertex lobed.

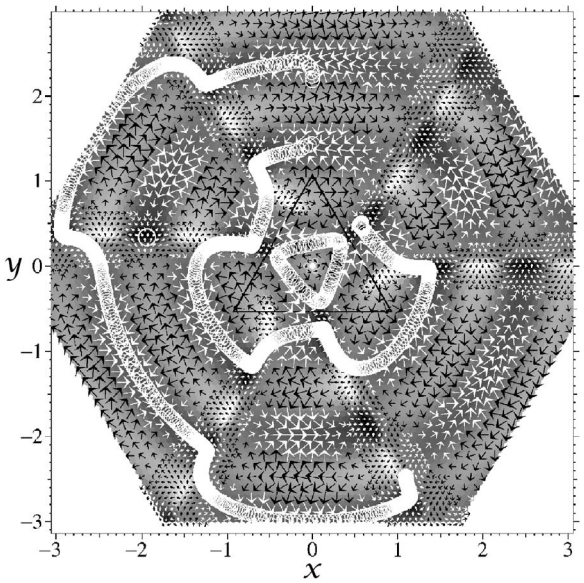

FIG. 2. Drift velocity plot for d=1.85. Tip trajectories follow (parts of) the first three stable limit cycles. The second and third are examples of vertex and lateral lobed limit cycles, respectively. The isolated circle marks the position of a stable focus.

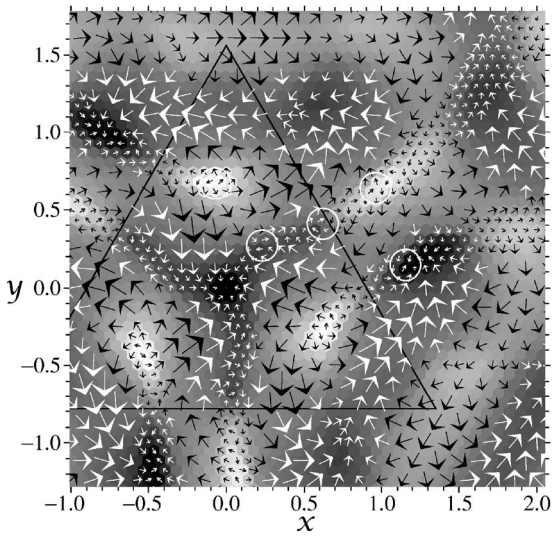

FIG. 3. Drift velocity plot for $d=2.70$. Selected fixed points referred to in the text are inside white circles.

The central stable limit cycle shrinks down to a stable focus (via a supercritical Hopf bifurcation) for $d \approx 2$. The parts of the innermost vertex lobed limit cycle get ever closer to the centroid as d increases. They are separated from the stable focus there by saddle nodes. At around $d=2.6$ the limit cycle is destroyed as a result of a homoclinic bifurcation and trajectories starting on the first VEZs end up at the centroid. As before, the extended basin of attraction for the central attractor only occurs for a narrow range of domain size. By $d=2.7$, trajectories starting on the first VEZ instead end up on a sink in the neighboring stagnation zone. Now that there are no longer any limit cycles in the domain, it is of interest to survey the fixed points present. Referring to the region $0 \leqslant \theta < 120°$ in Fig. 3, as well as the sinks at the centroid and the stagnation zone, there is an unstable node at (−0.07, 0.67) and a saddle node at (0.23, 0.27). These originated when the first unstable limit cycle broke around $d=1.82$. There is also a stable focus just inside the domain at (0.62, 0.41) and further out a saddle node at (0.96, 0.64). This pair of fixed points was created in a bifurcation inside a stagnation zone at around $d=2.57$. This lattice of evenly separated sources and sinks is reminiscent of the cellular structure seen for the square domain [11,12]. As in that case, more fixed points appear inside the domain as the domain size is increased still further.

The most important types of behavior seen in the computational study are confirmed by the results of our experiments with the light-sensitive BZ reaction. The increasingly triangular shape of the innermost limit cycle as it shrinks down to become a stable focus as d increases can be seen in the results shown in Figs. 4(a)–4(d). Figure 4(e) shows the spiral core first drifting clockwise as a result of starting close to an unstable limit cycle, and then reversing its sense as it approaches a stable limit cycle. Part of a lateral lobed limit cycle is clearly seen in Fig. 4(f). Notice the presence of the stagnation zone (where the loops are bunched together) at the start of the lobe.

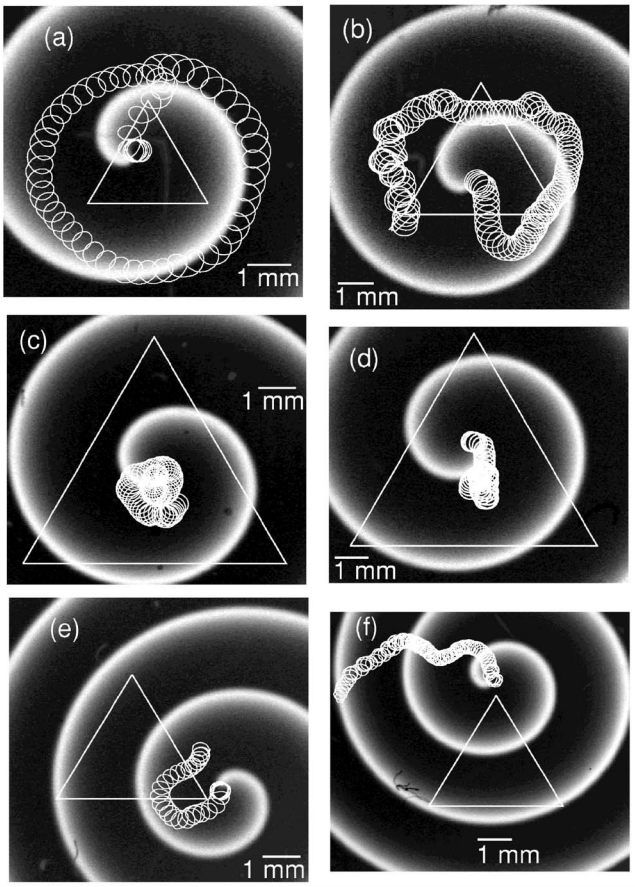

FIG. 4. Experimental results for various (d, k_{fb}): (a) (1.0, 0.6); (b) (1.3, 0.6); (c) (2.3, 1.0); (d) (2.5, 0.9); (e) (1.8, 0.6); (f) (1.8, 1.4). The spiral wave image is taken at the start of the tip trajectory. Feedback is initiated after a few revolutions of the tip.

IV. PLANE WAVE APPROXIMATION

We now turn our attention to the motion of the core when it is far from the domain. To explain features of the drift vector fields, we would ideally require an analytical expression for the drift velocity at each point. Two approaches have been suggested for obtaining this after assuming that the wave front takes the form of an Archimedean spiral [20]. The more direct method is to calculate $B(t)$ by finding the total length of the sections of an Archimedean spiral that lie inside the domain. Alternatively, the drift velocity at a point can be obtained by summing the drift vectors induced by each point inside the domain. For a triangular domain, such expressions cannot be written in closed form. However, since the curvature of a spiral wave decreases with increasing distance from the core, for sufficiently large core-domain distances we can treat the parts of the spiral wave inside the domain as a unit-wavelength plane wave train propagating away from the spiral core in the direction of the domain as illustrated in Fig. 5(a). As the tip rotates about the core once in time T, the plane wave fronts move forward one unit at uniform speed. In this plane wave approximation (PWA), we have $B(t) = L(p)/S$ where $L(p)$ is the sum of the lengths of the lines inside the domain and p is the distance from O to the nearest

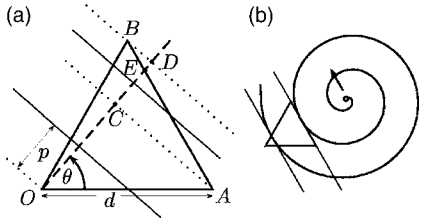

FIG. 5. Plane wave approximation. (a) Construction used to find $L(p)$. The spiral core is in the direction of the dashed line. Solid lines perpendicular to the dashed line are wave fronts. In (b) the small circle represents the spiral core and the arrow the current direction of motion of the tip.

plane wave in the direction of the spiral core. It therefore lies in the range $0 \leqslant p < 1$, and if time is scaled so that $T=1$, $p=(1-t+t_0) \bmod 1$ where t_0 is a time at which a plane wave passes through O. We only need to consider the cases $30° \leqslant \theta \leqslant 90°$ since, in addition to the threefold rotational symmetry, there is also reflection symmetry about the line $\theta=30°$. For $30° < \theta < 90°$, a wave front passing inside the domain either intersects OB and OA or OB and AB. The number of wave fronts that intersect OB and OA is the number M of wave fronts that lie between O and C, where point C lies on the dashed line in such a position that AC is perpendicular to OC. Then $M=[d \cos \theta - p + 1]$ where $[\cdot]$ represents the integer part. The remaining wave fronts that pass through the domain, and intersect OB and AB, lie between C and D. Point D lies on the dashed line in such a position that BD is perpendicular to OD. If N is the number of wave fronts between C and D then $M+N=[d \cos(60° - \theta) - p + 1]$. To find $L(p)$ we need to introduce a further point E which is the intersection of the dashed line with the line that passes through A and B. Then using simple geometry we obtain

$$L(p) = \sum_{m=0}^{M-1} (p+m)\{\tan\theta + \tan(60^\circ - \theta)\} + \sum_{m=M}^{M+N-1} (p+m)\tan(60^\circ - \theta) + \{OE - (p+m)\}\tan(120^\circ - \theta)$$

where the length OE is given by

$$OE = d\{\cos\theta + \sin\theta \tan(\theta - 30^\circ)\}.$$

It is apparent that, when $d \geqslant 2/\sqrt{3}$ and the plane wave fronts are parallel to one of the sides, $B(t)$ will take the form of a period-T sawtooth wave composed of one or two linear sections. The gradient of $B(t)$ will be positive or negative depending on whether the wave fronts enter at a vertex ($\theta \bmod 120° = 90°$) or side ($\theta \bmod 120° = 30°$) respectively. The sawtooth discontinuity corresponds to the wave front crossing one of the sides. Referring to Fig. 5(b) in which $\theta = 30°$ and the spiral core is a half integer number of wavelengths from the side of the triangle, as the spiral wave (approximated by a plane wave) crosses the side of the triangle, there will be a sudden increase in the excitability resulting in a boost to the motion of the tip and hence also the core in the direction shown. Now consider moving the spiral core a little further away from the domain. In order for the wave front to touch the side, the spiral must be rotated counterclockwise. Thus as the spiral core moves away from the domain, the drift velocity vectors rotate counterclockwise, completing one rotation every wavelength. The spiral core shown is therefore in the center of an attracting region. It is evident that the greatest difference between the maximum and minimum values of $B(t)$ will occur when the plane waves are aligned with a side. The magnitude of the first Fourier component and hence the drift velocity will be the largest in these cases. From the above it is now apparent that the spiral core in Fig. 5(b) is at the center of an attracting LEZ and that in general these are located at distances from the centroid of $m+\frac{1}{2}+d/\sqrt{12}$, where m is an integer.

The difference in drift directions between two points is given by the difference in phase between the first Fourier components of $B(t)$. The phase of this component is approximately $\pi/2$ behind (ahead of) the discontinuity of the negative (positive) gradient sawtooth wave described earlier. The net phase difference of π between the two cases results in the centers of attracting VEZs occurring at integer, rather than half-integer, distances from the side and hence their distance from the centroid is given by $m-d/\sqrt{12}$. These expressions explain why LEZs move away from the centroid while VEZs move toward it with increasing d. One also sees that since the switching between vertex and lateral lobed limit cycles described earlier for the region near the domain for $1.8 < d < 1.9$ results from the opposing directions of motion of the VEZs and LEZs, this switching phenomenon is generic for this system and will occur for domain sizes and distances from the centroid larger than this.

In Fig. 6 the PWA estimates for the positions of the express zones are compared with the measured values from the numerical calculation. As expected, the agreement is best far from the domain. Also, for a given distance the discrepancy is larger for LEZs than VEZs. This is because how well the plane wave approximates the spiral wave depends on the distance of the core to the side which will evidently be smaller for a LEZ than a VEZ for a given core-centroid distance.

The PWA can also be used to explain some features of the magnitudes of the drift vectors in the directions of the side midpoints and vertices. First, if the spiral core in the center of a VEZ or LEZ is moved directly away from the centroid, according to the PWA it will only result in a phase change in $B(t)$. Hence the magnitude of the drift vector in these directions should be constant. Note that this prediction is also true for the Archimedean spiral approximation. For the real spiral, it would not be expected to be constant due to the tip not remaining in the same place as the wave rotates. Second, the difference between the maximum and minimum total length of the plane wave fronts in the domain is d. Since the area of the domain is proportional to d^2, $B(t)$ and hence the drift velocity should be inversely proportional to d. As shown in Fig. 7, the measured range of drift vector amplitude A within an express zone is generally small. It is to be expected that this amplitude should be the same for VEZs and LEZs although this only appears to be the case near $d=2$. The am-

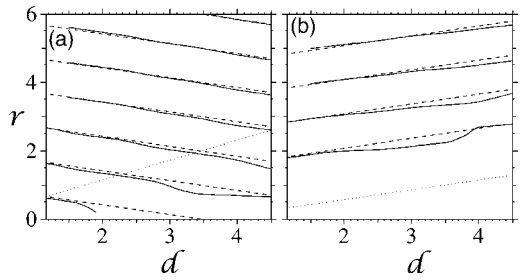

FIG. 6. Distances of centers of attracting express zones in the directions of (a) the vertices and (b) the midpoints of the sides. Solid lines, from computational results; dashed line, from PWA. The dotted lines show the edge of the domain.

plitudes certainly decrease with increasing d, but only approximately satisfy the inverse relationship obtained from the PWA.

We can also use the PWA to account for the occurrence, strength and positioning of the stagnation zones. When the plane waves are perpendicular to one of the sides, as is depicted in Fig. 5(a), the change in $B(t)$ and therefore magnitude of the drift velocity is minimized. If stagnation zones are present far from the domain, we therefore expect that they lie in the directions $\theta=n\pi/3$ away from the centroid. For plane waves traversing the domain in this way, it is easily seen that $B(t)$ will be constant (and hence the drift velocity zero) if there are always an even number of wave fronts in the domain, since for each wave front whose length inside the domain is increasing, there will be a corresponding one whose length is decreasing by the same amount. As a result, according to the PWA it would be expected that the stagnation zones far from the domain should be strongest when d is close to an even integer. On the other hand, if there are always an odd number of wave fronts in the domain, $B(t)$ will vary with the result that the drift speed will not be very small. Hence for d close to an odd integer we expect very weak stagnation zones. This is seen for $d=3$ in Fig. 8(a) in contrast to the very pronounced stagnation zones when d is close to an even integer as in Fig. 2 and Fig. 8(b). When $\theta=n\pi/3$, the PWA is at its crudest, and so the stagnation zones are only approximately in these directions.

Finally, it is worth noting that in the more extensive plots, far from the domain there is an additional symmetry about the directions $n\pi/3+\pi/6$. This is indicating that the lateral asymmetry of the spiral wave is no longer of importance at these distances.

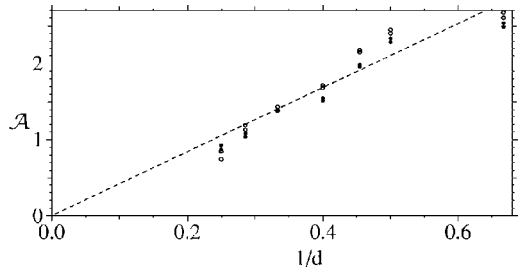

FIG. 7. $(1/d,A)$ plot of maximum and minimum drift vector amplitudes lying in the directions $\theta=30°$ (open circles) and 90° (filled circles) for the express zones at a distance of about 6 from the centroid. The dotted line passes through the value with the smallest range of amplitudes.

V. DISCUSSION

In the analysis of spiral wave dynamics under feedback control via an equilateral triangular domain, we have seen two basic types of behavior. First, trajectories beyond some critical distance from the centroid (this distance increasing with domain size) generally will be attracted to stable limit cycles. In contrast to the results from circular and square domains, both experimental measurements and computational calculations show that these will in general be lobed if the domain is sufficiently large. The plane wave approximation tells us that these lobed limit cycles will occur at arbitrarily large distances from the centroid and that as the domain size is increased, each limit cycle will only last for a limited range of d before being destroyed. Parts of the attracting regions making up such a destroyed limit cycle some distance from the domain will later join up to form a new limit cycle. Second, inside the domain, in particular for larger domain sizes, we see a regular array of stable and unstable fixed points.

The existence of express zones and stagnation zones is apparent in the experimental and numerical results of earlier studies, although only in a recent article on two-point feedback have regions of particularly low spiral-core drift velocity been commented upon [21]. In this case, infinitely long fixed lines emanating from the sensory region are embedded in stagnation zones. The zones are very extensive for some parameter values. The fixed lines (along which the drift velocity is exactly zero) resemble the lines of narrow stagnation zones we have found in the cases when d is close to an even integer.

In the control of a spiral wave both types of zone are of great importance. If a spiral tip is to be moved from one region to another, like stable fixed points, stagnation regions are to be avoided. Conversely, rapid movement of the spiral core could be achieved by choosing a path composed of express zones.

The stagnation zones we have reported here are not unique to feedback via triangular domains. Using the PWA it

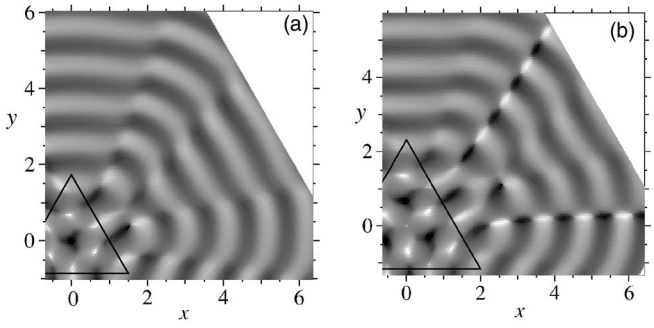

FIG. 8. Inverse-magnitude scaled divergence plots for $d=$(a) 3.0 and (b) 4.0.

can be seen that they would be expected to occur, for instance, aligned with the vertices of a square domain and be the most prominent when $d=\sqrt{2}n$. From Fig. 2(d) in Ref. [12] it is apparent that they do. It is also straightforward to understand why the very extended stagnation zone occurs in the case of the rhombus shaped sensory domain in their Fig. 1(g).

The calculations and experiments were performed for rigidly rotating spiral waves. For meandering spirals, there is a significant deviation from an Archimedean form near to the spiral core. However, this is no longer the case several wavelengths away from the core. After averaging over the meandering motion, it is to be expected that the corresponding results for meandering spirals would be qualitatively similar, as has been shown to be the case in both experimental studies and theoretical predictions using the spiral wave approximation for feedback systems using other domain shapes [20].

The PWA approach introduced here was presented with the caveat of only applying far from the domain. Nevertheless, it is of note that some of its predictions for the drift vector field, such as the location of the express zone centers, are also reasonably accurate quite near the domain. We used the PWA for the directions $\theta=n\pi/6$ since they turn out to correspond to the centers of express or stagnation zones and the expressions for $B(t)$ in these cases are the most straightforward to analyze. Applying our PWA techniques and their extension through examining the case for other angles to explain features of drift vector fields for this and other domain geometries is an interesting topic for future investigation.

ACKNOWLEDGMENTS

S.N. thanks the Graduiertenföderung and Neuroverbund Projekt des Landes Sachsen-Anhalt for financial support. M.A.A. thanks the Biophysics Department, Otto-von-Guericke University for their hospitality during his visit.

[1] A. T. Winfree, Science **175**, 634 (1972).
[2] S. Jakubith, H. H. Rotermund, W. Engel, A. von Oertzen, and G. Ertl, Phys. Rev. Lett. **65**, 3013 (1990).
[3] F. Siegert and C. J. Weijer, J. Cell. Sci. **93**, 325 (1989).
[4] J. M. Davidenko, A. V. Pertsov, R. Salomonsz, W. Baxter, and J. Jalife, Nature (London) **355**, 349 (1992).
[5] X. Huang, W. C. Troy, Q. Yang, H. Ma, C. R. Laing, S. J. Schiff, and J.-Y. Wu, J. Neurosci. **24**, 9897 (2004).
[6] V. S. Zykov, Biofizika **31**, 862 (1986).
[7] O. Steinbock, V. S. Zykov, and S. C. Müller, Nature (London) **366**, 322 (1993).
[8] S. Grill, V. S. Zykov, and S. C. Müller, J. Phys. Chem. **100**, 19082 (1996).
[9] S. Kantrasiri, P. Jirakanjana, and O.-U. Kheowan, Chem. Phys. Lett. **416**, 364 (2005).
[10] V. S. Zykov, O.-U. Kheowan, O. Rangsiman, and S. C. Müller, Phys. Rev. E **65**, 026206 (2002).
[11] V. Zykov and H. Engel, Phys. Rev. E **70**, 016201 (2004).
[12] O.-U. Kheowan, S. Kantrasiri, P. Wilairat, U. Storb, and S. C. Müller, Phys. Rev. E **70**, 046221 (2004).
[13] O.-U. Kheowan, V. Zykov, and S. C. Müller, Phys. Chem. Chem. Phys. **4**, 1334 (2002).
[14] O.-U. Kheowan, S. Kantrasiri, C. Uthaisar, V. Gáspár, and S. C. Müller, Chem. Phys. Lett. **389**, 140 (2004).
[15] D. Barkley, Physica D **49**, 61 (1991).
[16] V. S. Zykov and S. C. Müller, Physica D **97**, 322 (1996).
[17] V. S. Zykov and H. Engel, Phys. Rev. E **66**, 016206 (2002).
[18] S. Grill, V. S. Zykov, and S. C. Müller, Phys. Rev. Lett. **75**, 3368 (1995).
[19] O.-U. Kheowan, Ph.D. thesis, Mahidol University, 2001 (unpublished).
[20] V. Zykov and H. Engel, Physica D **199**, 243 (2004).
[21] V. S. Zykov, H. Brandtstädter, G. Bordiougov, and H. Engel, Phys. Rev. E **72**, 065201(R) (2005).